SUPPLEMENTAL INFORMATION APPENDIX

Title: Clustering of mammalian *Hox* genes with other H3K27me3 targets within an active nuclear domain

Running title: *Hox* genes and H3K27me3 clustering

Authors: Maxence Vieux-Rochas[1], Pierre J. Fabre[1], Marion Leleu[1], Denis Duboule[1,2], Daan Noordermeer[1]

Affiliations: [1] School of Life Sciences, Swiss Federal Institute of Technology – Lausanne (EPFL), 1015 Lausanne, Switzerland

[2] Department of Genetics and Evolution, University of Geneva, Sciences III, 1205 Geneva, Switzerland

Contents:

Full Methods

Animal care, tissue sampling and ES cell culture

All experiments were performed in agreement with the Swiss law on animal protection (LPA) with the appropriate legal authorizations to D.D. Tissue samples were isolated at embryonic day 10.5 (E10.5), with day E0.5 being noon on the day of the vaginal plug. Individual homozygous Inv(*Itga6-HoxD*^{RVIII}) E10.5 forebrains were obtained by crossing heterozygous mice (1). Homozygous control E10.5 forebrains obtained from the same crosses were used as wild-type controls. Genotyping using standard PCR protocols was done on material remaining after isolation of forebrain samples.

Mouse ES cells (for FISH studies) were grown under feeder-free conditions on gelatinized plates in Dulbecco's modified Eagle's medium (DMEM, Life Technologies) supplemented with 17% fetal calf serum, 1x non-essential amino acids (Life Technologies), 1x Pen – Strep (Life Technologies), Sodium Pyruvate (Life Technologies), 0.1 mM β-mercaptoethanol, and 1000 U/ml LIF.

4C-sequencing

Fragments of tissues for 4C-sequencing were isolated in PBS, transferred into PBS supplemented with 10% Fetal Calf Serum, incubated for 45 minutes with 1 mg/ml collagenase (Sigma) and made single cell using a cell strainer (BD Falcon). Chromatin fixation, cell lysis and 4C-library preparation were done as previously described with *NlaIII* (New England Biolabs) as the primary restriction enzyme and *DpnII* (New England Biolabs) as the secondary restriction enzyme (2). E10.5 forebrain 4C-seq samples (control and homozygous inversion samples) consisted of 13-18 dissected forebrains pooled after genotyping. E10.5 maxillary arch and junction 4C-seq samples consisted of pools of 76 fine-dissected tissue samples. The ES cell 4C-seq library sample was generated as part of a previous study (3).

For each viewpoint, a total of 800 ng of each 4C-seq library was amplified using 16 individual PCR reactions with inverse primers including Illumina Solexa adapter sequences (primer sequences in Table S1). Illumina sequencing was done on multiplexed samples, containing PCR amplified material of up to eight viewpoints, using 100 bp single end reads on the Illumina HiSeq system according to the manufacturer's specifications.

Newly generated 4C-seq data sets (E10.5 forebrain data for viewpoints on chromosome 2 (both control and inverted *HoxD* cluster viewpoints), E10.5 maxillary arch and E10.5 junction cells data and non-*HoxD* cluster viewpoints in ES cells) and previously generated data sets (E10.5 forebrain data for *HoxC*, *HoxB* and *HoxA* cluster viewpoints; (2), E10.5 anterior trunk data (2) and *Hox*-cluster ES cell data (3) were all mapped and translated into restriction fragments using the 4C-seq pipeline of the BBCF HTSstation (2, 4), available at http://htsstation.epfl.ch, according to ENSEMBL Mouse assembly NCBIM37 (mm9). For visualization within four Mb (megabase) large windows, 4C-seq data was smoothed using a running mean with window size of 11 fragments.

Unprocessed 4C-seq data is available from the Gene Expression Omnibus (GEO) repository under accession numbers GSE61372 and GSE55344.

ChIP-sequencing

Embryonic tissues for ChIP-seq were dissected into PBS, transferred to PBS supplemented with 10% Fetal Calf Serum and incubated for 45 minutes with 1 mg/ml collagenase (Sigma). Cells were fixed for 5 minutes in a 2% formaldehyde solution at room temperature. E10.5 forebrain ChIP-seq samples (control and homozygous inversion samples) consisted of eight to ten dissected forebrains pooled after genotyping. E10.5 maxillary arch and junction ChIP-seq samples consisted of 125 fine-dissected tissue samples. ChIP-seq samples were fragmented to a range of 200-500 bp using either tip sonication (E10.5 forebrain; Misonix S4000) or waterbath sonication (E10.5 junction and maxillary arch; Diagenode Bioruptor). For all ChIP assays, 10 µg of cross-linked chromatin was immunoprecipitated as previously described (2) using an anti-Histone H3K27me3 (17-622, Millipore) antibody. ChIP-seq libraries were constructed from 6 to 10 ng of immune-precipitated DNA according to the manufacturers instructions (Illumina). Sequencing was done using 50 or 100 bp single end reads on the Illumina HiSeq system according to the manufacturer's specifications. ChIP-seq reads (including previously generated data sets described in supplemental data file S8) were mapped to ENSEMBL Mouse assembly NCBIM37 (mm9), and extended to 100 bp if read lengths smaller than 100 bp were used, using the ChIP-seq pipeline of the BBCF HTSstation (4), available at http://htsstation.epfl.ch. Newly generated ChIP-seq data is available from the Gene Expression Omnibus (GEO) repository under accession number GSE61372.

Re-analysis of published HiC and LaminB1 data

Normalized HiC matrices at 40 kb resolution from mouse ES cells and cortex cells (5, 6) were obtained from http://yuelab.org/hi-c/download.html. Interaction matrices for TADs and interactions within a four Mb window were obtained using standard settings on the previously mentioned website, or using the indicated sensitized cut-offs. To calculate for the presence of HiC compartments, the observed/expected value and Pearson correlation for each 40 kb bin was calculated similar to a previously published HiC study on human lymphoblastoid cells (7). Subsequently, the principal component (represented by the eigenvector) was calculated at a resolution of one Mb (i.e. after binning of 25 consecutive bins), 400 kb (binning of 10 consecutive bins) or 80 kb (binning of two consecutive bins). The first three Mb of Mouse assembly NCBIM37 (mm9) are empty, which results in an artificially high value for the first data containing bin in the principal component analysis. Prior to calculating the principal component, we therefore excluded the first 3 Mb + the first data bin. After calculation of the principal component, the sign of the eigenvector for each data set, resolution and chromosome was determined manually by comparing to gene density and H3K4me3 ChIP-seq data. For each chromosome, the sign of the eigenvector for the active, gene rich compartment (compartment A) was set to positive and the sign of the eigenvector for the inactive, gene poor compartment (compartment B) was set to negative. Constitutive HiC compartments at 400 kb resolution were determined by intersecting mouse ES cell and cortex cell data and are given in File S5.

LaminB1 data from mouse ES cells, NPC cells, astrocytes and MEFs, as determined by DamID experiments, were obtained from a previously published study (8) (see supplemental data file S8). Probe values from individual replicates were averaged and translated to genomic position without further post-processing. Coordinates for constitutive LADs and iLADs were previously reported (9) (see this appendix, Table S2).

To correlate HiC and LaminB1 data, for each HiC data bin (at resolutions of 1 Mb, 400 kb and 80 kb) the mean LaminB1 probe signal per cell type of all probes within the bin was determined. Next, the spearman correlation was determined between the eigenvector of each HiC bin and the mean signal intensity of LaminB1 data within the same bin.

3D DNA-FISH and Immuno-FISH

3D DNA Fluorescent in-situ hybridization was conducted as described previously (10). E10.5 mouse embryos were fixed in 4% paraformaldehyde, embedded in paraffin blocks and cut in 6 μm thick slices. ES cells were fixed with 4% paraformaldehyde for 10 minutes. Probes were prepared by nick-translation with biotin- or digoxigenin-UTP using fosmid and BAC clones obtained from BACPAC Resources Center (https://bacpac.chori.org/) and listed in Table S1. 100 ng (fosmid) or 200 ng (BAC) of probes were used with 7 μg of Cot1-DNA and 10 μg of sonicated salmon sperm DNA. For immuno-FISH, immunohistochemistry was performed using the anti-LaminB1 primary antibody (ab16048, Abcam) followed by a secondary goat anti-rabbit antibody labeled with Alexa Fluor 488 (A21206, Life Technologies) prior to the 3D-FISH experiment. Slides were stained with DAPI and mounted in ProLong Gold (Life Technologies). Images were acquired using a B/W CCD ORCA ER B7W Hamamatsu camera on an inverted Olympus IX81 microscope. The image stacks with a 200 nm step were saved as TIFF stacks. Image reconstruction and deconvolution were performed using FIJI (NIH, ImageJ v1.47q) and Huygens Remote Manager (Scientific Volume Imaging, version 3.0.3). Distance measurements between probe signals were determined using an automated spot detection algorithm followed by visual verification and manual correction (IMARIS version 6.5, Bitplane AG and Matlab 7.5, MathWorks SA). Nuclear position measurements were done manually using IMARIS (version 6.5, Bitplane AG). Statistical significance of distances and nuclear position were performed using an unpaired two-sample t-test. Statistical significance of distances to *Hoxd13* was determined using the Kruskal-Wallis test followed by Dunn's post test.

Construction and correlation of domainograms

To detect ultra-long range intra-chromosomal and inter-chromosomal interactions in a reliable manner and to asses the significance of H3K27me3-marked genomic regions, we used a previously described domainogram analysis based on enrichment within multiscale windows (e.g. (11-13). For improved sensitivity, intra-chromosomal 4C-seq domainograms were calculated separately for sequences upstream and downstream of the viewpoints using window sizes ranging from 1 to 200 valid *NlaIII* restriction fragments. For inter-chromosomal 4C-seq analyses, domainograms were calculated for each

chromosome separately using window sizes ranging from 1 to 200 valid *NlaIII* restriction fragments. To allow maximum comparability between 4C-seq data and ChIP-seq data, we first translated ChIP-seq data to 4C-seq resolution: for each valid *NlaIII* fragment, the mean ChIP-seq data value was determined and subsequently domainograms were calculated for each chromosome separately using window sizes ranging from 1 to 200 valid *NlaIII* restriction fragments. For both 4C-seq and ChIP-seq data, BRICKs (Blocks of Regulators In Chromosomal Kontext) were determined by scoring for the highest significance of enrichment within the window size of 1 to 200 fragments (11). For 4C-seq experiments, a cut-off for significance of $p < 10^{-3}$ was used, with strongly enriched clustering of signal in the five Mb upstream and downstream of the viewpoint ignored. For ChIP-seq experiments, a cut-off for significance of $p < 10^{-6}$ was used. Depending on the figure, only BRICKs with significance $p < 10^{-6}$ or $p < 10^{-10}$ are shown. 4C and ChIP-seq BRICKs are provided in supplemental data files S1-S4.

Enrichment of 4C BRICKs amongst the most significant H3K2me3 BRICKs (K27 BRICKs) was determined by scoring the most significant K27 BRICK that (partially) overlaps each 4C BRICK. Correlation between 4C or ChIP-seq BRICKs and HiC compartments was determined by scoring the HiC eigenvector of the bin that covers the 4C or ChIP-seq BRICK. Correlation between 4C or ChIP-seq BRICKs and LADs/iLADs was determined by taking the mean of all LaminB1 probes within the region covered by the 4C-seq or ChIP-seq BRICK. The significance of the difference between correlations was determined using a two-sided t-test.

Determination of global 4C-seq scaling factors

Global scaling factors in 4C-seq data, which are conceptually similar to the power law scaling analyses presented in (7) and (14), were determined on the longest stretch of continuous intra-chromosomal data for each viewpoint: upstream and downstream for viewpoints on chromosome 2 (minimum 68 Mb distance), upstream for viewpoints in the *HoxC* and *HoxB* clusters (minimum 100 Mb and 93 Mb distance) and downstream of the *HoxA* cluster (minimum 97 Mb distance). Signal within bins of 0.1 log(10) distance from the viewpoint was pooled, starting at logarithmic bin 4.5 (31.6 kb from viewpoint) up to the furthest bin fully covered by the data (typically bin 7.8 to 8.0 or 63 Mb to 100 Mb). Subsequently, total signal was divided by the (linear) size of the bin, and data was plotted as a product of the log(10) distance from the viewpoint versus the log(10) of the relative contribution to the total signal. The resulting graphs follow a typical shape that is also observed in HiC experiments, with a more plateau phase at short and long distances and a steeper gradient at intermediate distance. As we were not interested in understanding overall patterns of chromatin organization (see e.g. (7, 14), but rather wanted to score for global differences between early embryonic ES cells and later stage E10.5 forebrain cells, and between H3K27me3 and non-H3K27me3-marked viewpoints, we decided to determine scaling factors over the longest possible range. Scaling factors for each individual viewpoint (per cell type), and for combined viewpoints per chromosome (and cell type) were therefore determined by fitting a linear (first degree polynomial) line over the full range of the data. Though we detected

considerably different scaling factors for each chromosome over this range (similar to (14) but independent of the presence of the H3K27me3 mark), we find that the global scaling factor for each viewpoint in ES cells has a consistently larger negative value than its counterpart in E10.5 forebrain cells, with intersection typically around 1 to 2 Mb from the viewpoint.

Determination of enrichment of 4C-seq signal in K27 BRICKs

Enrichment of 4C-seq signal in K27 BRICKs was determined by scoring the number of positive intra-chromosomal 4C fragments > 5 Mb away from the viewpoint for overlap with K27 BRICKs. The number of positive fragments was then corrected for the genomic coverage of K27 BRICKs within the remainder of chromosome 2 and the enrichment *versus* all fragments on chromosome 2 was calculated. To normalize between data sets, the enrichment was divided by the average for all viewpoints in the analysis, including the two control loci.

Supplemental figures

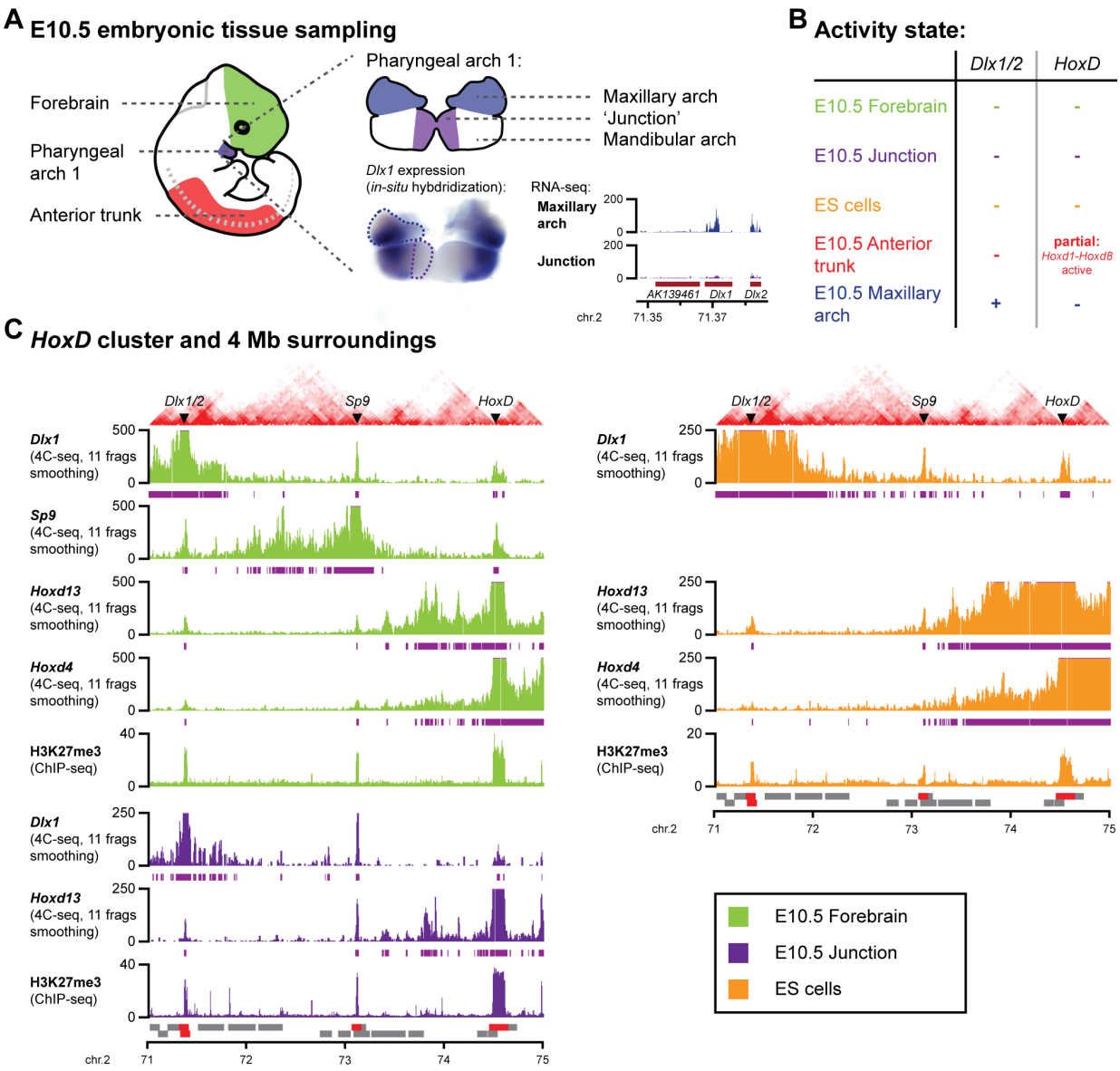

Figure S1. The H3K27me3-marked *HoxD* cluster and neighboring *Dlx1/2* and *Sp9* H3K27me3-marked genes interact with one another, despite being located in different TADs.

(A) Origin of micro-dissected tissues at day 10.5 (E10.5) mouse embryos. Activity of the *Hoxd* and *Dlx1/2* genes in E10.5 forebrain and anterior trunk samples was described previously (2). The magnification on the right shows a frontal view of the first pharyngeal arch, with the maxillary and mandibular parts and in magenta the distal 'junction' region between both aspects of the mandibular arch. The first pharyngeal arch, encompassing both the maxillary and mandibular arches, is devoid of *Hox* gene activity (15). In contrast, a previous study detected strong *Dlx1* signal in the maxillary arch at day E11.5, whereas the mandibular arch consisted of two populations, with the median cells that constitute the junction being devoid of *Dlx1* signal (16). Similarly, at E10.5 this junction region is devoid of *Dlx1* transcripts, as shown below by *in-situ* hybridization and RNA-seq. Dashed lines depict the areas dissected for 4C-seq, ChIP-seq and RNA-seq. We used maxillary arch material as a rather homogenous source of cells positive for *Dlx1/2* transcripts, whereas the 'junction' cells that are located nearby and of similar origin, are used as negative for these two genes.

(B) Summary table of *Dlx1/2* and *HoxD* cluster transcriptional activities in the various cell types and tissues used in this study.

(C) Smoothed 4C-seq signal in a 4 Mb interval on chromosome 2 identifies long-range interactions between the H3K27me3-marked *Dlx1*, *Sp9*, *Hoxd13* and *Hoxd4* genes in multiple tissues. The purple bars below the 4C-seq profiles indicate signal with values within the 80% percentile (60% for ES cells). The positions of the *Dlx1/2* cluster, the *Sp9* gene and the *HoxD* cluster are indicated on top (black arrowheads), combined with HiC data obtained in ES cells (5), which, indicate the distribution of Topological Associated Domains (TADs). Despite being located in clearly different TADs, these H3K27me3-marked viewpoints thus interact among each other over long distances. 4C viewpoints are indicated on the right and genomic position and genes are indicated below, with the *Dlx1/2* cluster, the *Sp9* gene and the *HoxD* cluster indicated in red.

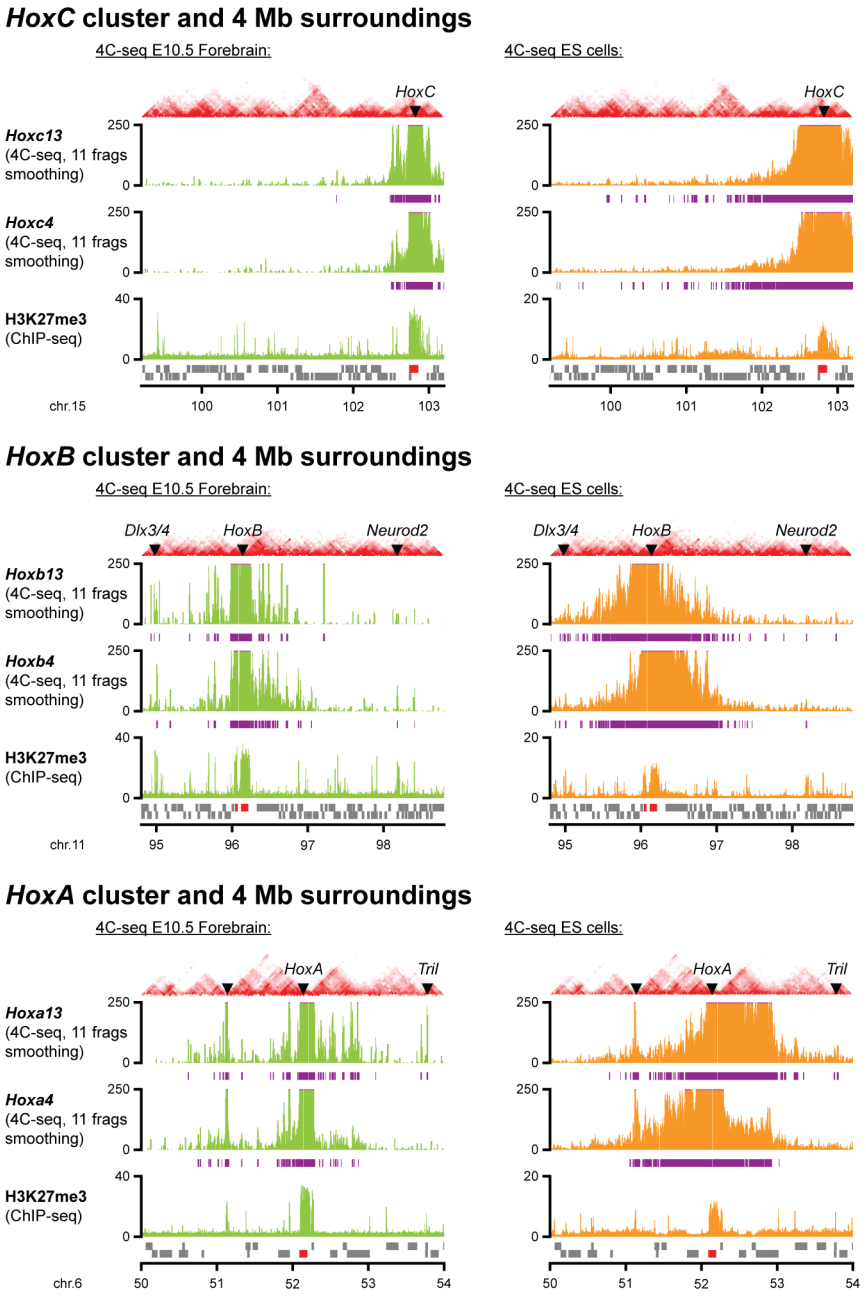

Figure S2. The *HoxB* and *HoxA* clusters interact with nearby H3K27me3-marked genes located in different Topological Associated Domains.

Smoothed 4C-seq profiles in a 4 Mb large interval around the *HoxC*, *HoxB* and *HoxA* clusters. The *HoxB* and *HoxA* clusters, but not *HoxC*, interact with nearby H3K27me3-marked genes in E10.5 forebrain and ES cells. Purple bars below the 4C-seq profiles indicate signal with values within the 80% percentile (E10.5 forebrain) or 60% percentile (ES cells). Selected positive interacting genes are indicated on top (black arrowheads), combined with HiC data from ES cells (5), to show the position of Topological Associated Domains (TADs). The 4C viewpoints are indicated on the right and genomic positions as well as genes are indicated below, with the *Hox* clusters in red.

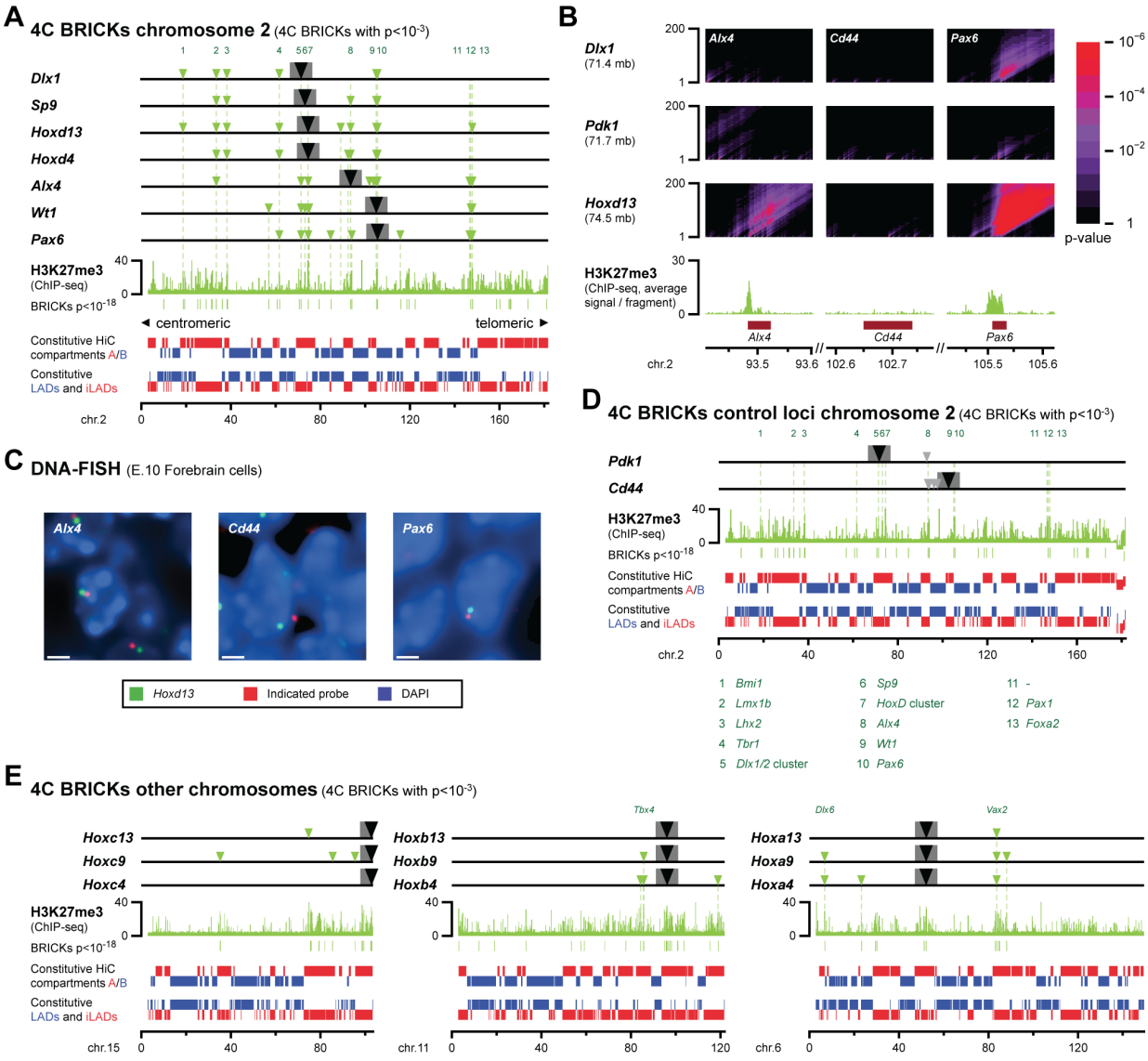

Figure S3. All four *Hox* clusters are involved in a network of intra-chromosomal H3K27me3-associated interactions within an active nuclear compartment.

(A) Linear visualization of long-range intra-chromosomal 4C-seq interactions by using seven H3K27me3-marked viewpoints on chromosome 2 in E10.5 forebrain cells. The seven viewpoints are involved in a recurring network of interactions with each other, as well as with other distant H3K27me3-marked loci (significant 4C BRICKs; see supplemental data file S1) that are primarily located within the constitutive HiC compartment A (positive red signal) and iLADs (negative red signal). The position of 13 recurring interacting H3K27me3-marked genes is indicated on top, with their names provided below in panel (D). The locations of the viewpoints are indicated by arrowheads and 5 Mb large regions upstream and downstream of each viewpoint are indicated by a grey box. H3K27me3 ChIP-seq signal and the most significant enriched regions (BRICKs with p-value $< 10^{-18}$) and genomic positions are indicated below.

(B) Magnification within a 200 kb large interval on the 4C-seq domainogram in E10.5 forebrain, for both the H3K27me3-marked *Dlx1* and *Hoxd13* viewpoints and the interspersed, non-H3K27me3-marked, *Pdk1* viewpoint. Long-range interactions of the H3K27me3-marked viewpoints precisely stem from distant H3K27me3-marked domains (the *Pax6* locus for both the *Dlx1* and *Hoxd13* viewpoints, and the *Alx4* locus for the *Hoxd13* viewpoint), whereas significant signal is detected neither for the *Pdk1* viewpoint, nor for the distant non-H3K27me3-marked *Cd44* domain.

Viewpoints and their approximate genomic location of chromosome 2 are indicated on the right and genomic positions and H3K27me3 signal on distant interacting loci are indicated below.

(C) Examples of DNA-FISH experiments used to determine the distribution of distances between the *Hoxd13* locus and indicated genes (colors as indicated in the legend) in E10.5 forebrain cells. Size bars = 2 μm.

(D) Two non-H3K27me3-marked control promoter viewpoints on chromosome 2 show few long-range interactions in E10.5 forebrain, with overlap neither amongst each other, nor with H3K27me3-marked loci. 13 recurrent interacting H3K27me3-marked genes are indicated below.

(E) Linear visualization of long-range intra-chromosomal 4C-seq interactions with three viewpoints in each of the other *Hox* clusters in E10.5 forebrain cells (significant 4C BRICKs; see supplemental data file S1). The viewpoints in each *Hox* cluster contact multiple H3K27me3-marked loci on the same chromosome in *cis*, which are generally located within the constitutive HiC compartment A (represented by positive red signal) and iLADs (represented by negative red signal). The names of recurring interacting H3K27me3-marked genes is indicated on top. The location of viewpoints is indicated by arrowheads and the regions spanning five Mb upstream and downstream of each viewpoint are indicated by a grey box. The genomic positions are indicated below.

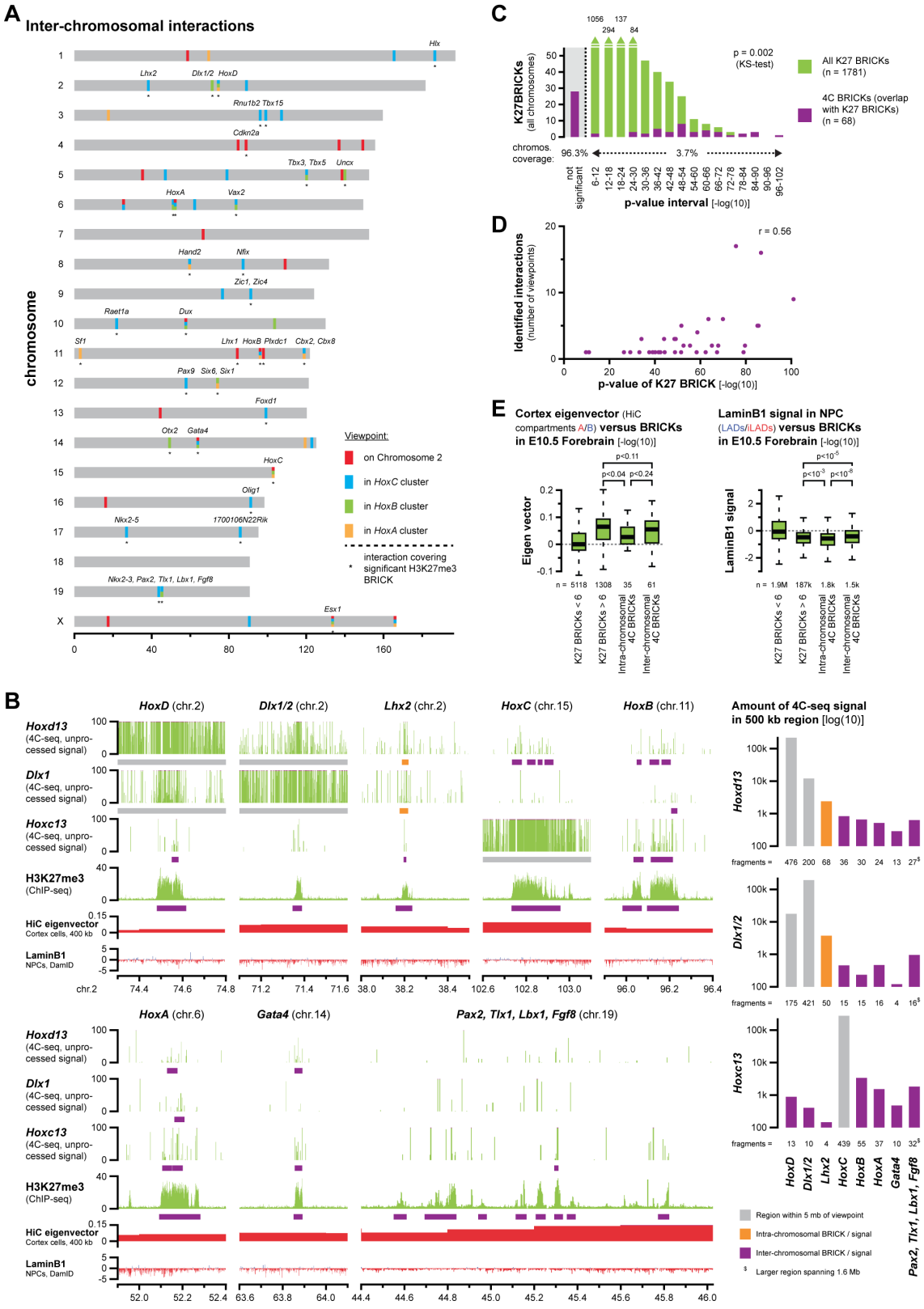

Figure S4. Significant H3K27me3-marked regions on different chromosomes interact within the active nuclear compartment, but at lower frequency than intra-chromosomal regions.

(A) Inter-chromosomal interactions (significant inter-chromosomal 4C BRICKs; see supplemental data file S2) for viewpoints on chromosome 2, as well as for the other *Hox* clusters in E10.5 forebrain cells. Color-coding is used to indicate the chromosomal position of the viewpoint(s). Inter-

chromosomal interactions that cover significant H3K27me3-marked regions are indicated with an asterisk below, and developmental regulatory genes present in such regions are shown above. The chromosomal positions are indicated below.

(B) Examples of raw intra- and inter-chromosomal 4C-seq signal for the *Hoxd13*, *Dlx1* and *Hoxc13* viewpoints in E10.5 forebrain cells at various locations in the genome (500 kb regions, including all *Hox* clusters). Below are given the H3K27me3 ChIP-seq signal in E10.5 forebrain cells, the HiC eigenvector in Cortex cells and the LaminB1 signal in NPCs Significant BRICKs are given below the 4C-seq and ChIP-seq patterns, using the color code provided at the bottom right. On the right, the total 4C-seq signal within the 500 kb regions is quantified (log(10) scale), with the number of positive fragments within this region provided below. Even though significant inter-chromosomal BRICKs are detected, their total signal is in the range of one to multiple orders of magnitude lower than intra-chromosomal interactions, similar in range to previously determined global genome interaction characteristics (7).

(C) Similar to intra-chromosomal long-range interactions, inter-chromosomal interactions are significantly enriched amongst the most significant H3K27me3-marked regions (K27 BRICKs).

(D) The significance of H3K27me3-marked regions directly correlates with the number of viewpoints that detect an inter-chromosomal interaction within these regions.

(E) Similar to intra-chromosomal interactions and significant H3K27me3-marked regions, inter-chromosomal interactions are enriched within the active HiC nuclear compartment A and iLADs.

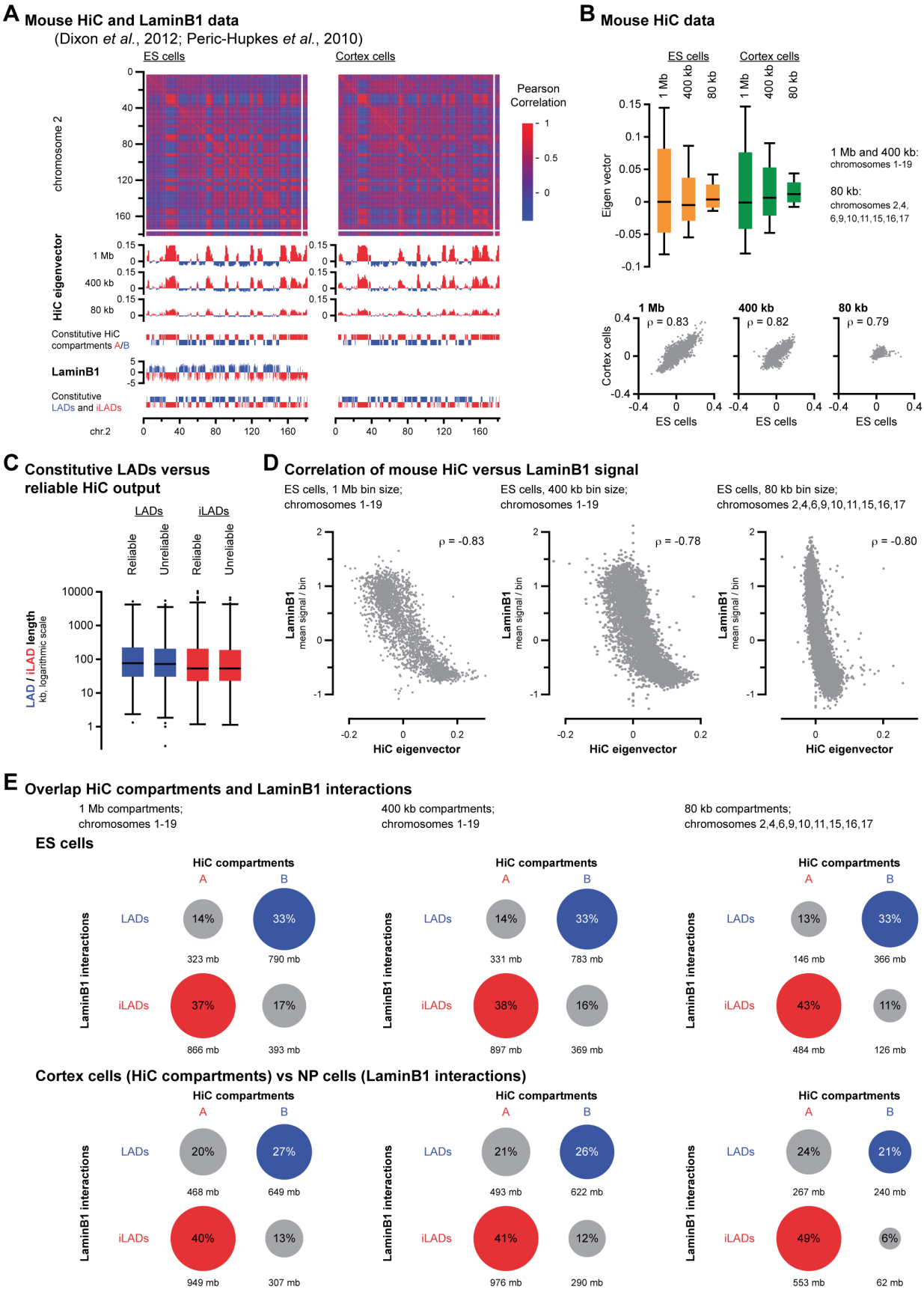
A Mouse HiC and LaminB1 data
(Dixon et al., 2012; Peric-Hukes et al., 2010)
ES cells
Cortex cells
Pearson Correlation
chromosome 2
HiC eigenvector
1 Mb
400 kb
80 kb
Constitutive HiC compartments A/B
LaminB1
Constitutive LADs and iLADs
chr.2
B Mouse HiC data
Eigen vector
1 Mb and 400 kb: chromosomes 1-19
80 kb: chromosomes 2,4,6,9,10,11,15,16,17
Cortex cells
ES cells
ρ = 0.83
ρ = 0.82
ρ = 0.79
C Constitutive LADs versus reliable HiC output
LADs
iLADs
Reliable
Unreliable
LAD / iLAD length
kb, logarithmic scale
D Correlation of mouse HiC versus LaminB1 signal
ES cells, 1 Mb bin size; chromosomes 1-19
ES cells, 400 kb bin size; chromosomes 1-19
ES cells, 80 kb bin size; chromosomes 2,4,6,9,10,11,15,16,17
ρ = -0.83
ρ = -0.78
ρ = -0.80
LaminB1 mean signal / bin
HiC eigenvector
E Overlap HiC compartments and LaminB1 interactions
1 Mb compartments; chromosomes 1-19
400 kb compartments; chromosomes 1-19
80 kb compartments; chromosomes 2,4,6,9,10,11,15,16,17
ES cells
HiC compartments
A
B
LaminB1 interactions
LADs
iLADs
14%
33%
323 mb
790 mb
37%
17%
866 mb
393 mb
14%
33%
331 mb
783 mb
38%
16%
897 mb
369 mb
13%
33%
146 mb
366 mb
43%
11%
484 mb
126 mb
Cortex cells (HiC compartments) vs NP cells (LaminB1 interactions)
20%
27%
468 mb
649 mb
40%
13%
949 mb
307 mb
21%
26%
493 mb
622 mb
41%
12%
976 mb
290 mb
24%
21%
267 mb
240 mb
49%
6%
553 mb
62 mb

Figure S5. Global patterns of HiC interactions are a proxy for interactions with the nuclear lamina.

(A) Example of re-assessed HiC data in ES and cortex cells (5, 6) on mouse chromosome 2 and its visual match with mouse LADs/iLADs (8, 9) (see supplemental data file S8 for the sources of external datasets). On the top, matrices with Pearson correlation of HiC data at a 40 kb resolution for ES (left) and cortex (right) cells, as obtained after normalization using a previously published strategy (7). Below the matrices, displayed from top to bottom, are the eigenvector of the principal component of the HiC data at three different resolutions (1 Mb, 400 kb and 80 kb, with the active compartment A in red and inactive compartment B in blue), the constitutive HiC compartments at a 400 kb resolution (based on overlaying the ES cell and cortex HiC data), the LaminB1 enrichment data (ES cell only) and constitutive LADs (blue, inactive) and iLADs (red, active). Genomic positions are indicated below. A visual inspection of HiC compartments and Lamin1B interactions revealed a large overlap, both between different cell types and between HiC and DamID data.

(B) Mouse HiC eigenvector and compartments are largely constitutive between ES and cortex cells. Top: distribution of HiC eigenvector value for different resolutions. For the 1 Mb and 400 kb resolutions, all autosomes are included. The calculation of the HiC eigenvector at 80 kb resolution was unreliable for many chromosomes (in most cases for both ES and cortex cells), resulting in all eigenvectors on these chromosomes carrying either a positive or negative sign. To avoid such normalization problems, we limited the analysis at 80 kb to the 9 indicated chromosomes that displayed consistent signals in both cell types. Bottom: correlation between HiC eigenvector in ES and cortex cells at different resolutions. The very high spearman correlation confirms a significant degree of similarity in HiC compartment organization between both ES and cortex cells.

(C) The size distribution of active and inactive domains (determined using LADs and iLADs as proxy) does not drastically differ on chromosomes with reliable and unreliable HiC eigenvectors at 80 kb resolution.

(D) Mouse HiC eigenvector and LaminB1 signals are anti-correlated, indicating that they refer to the same biological structure. Correlation of mouse HiC eigenvector at resolutions of 1 Mb, 400 kb and 80 kb versus LaminB1 signal (mean signal/HiC bin) in ES cells. For all three HiC resolutions, the presence in the active HiC compartment A (positive eigenvector) coincides with the presence in iLADs (negative, depleted LaminB1 signal), whereas the presence in the inactive HiC compartment B coincides with the presence in the repressive LADs. For the 1 Mb and 400 kb resolutions, all autosomes are included in the analysis, whereas for the 80 kb analysis, only the nine chromosomes with reliable eigenvectors are included.

(E) The HiC compartment A, at one Mb, 400 kb and 80 kb resolutions, primarily overlaps with iLADs, whereas the compartment B overlaps with LADs. For the 1 Mb and 400 kb resolutions, all autosomes are included in the analysis, whereas for the 80 kb analysis only the nine chromosomes with reliable eigenvectors are included. LaminB1 interacting regions are determined from raw DamID data (microarray enrichment over input) without filtering or smoothing.

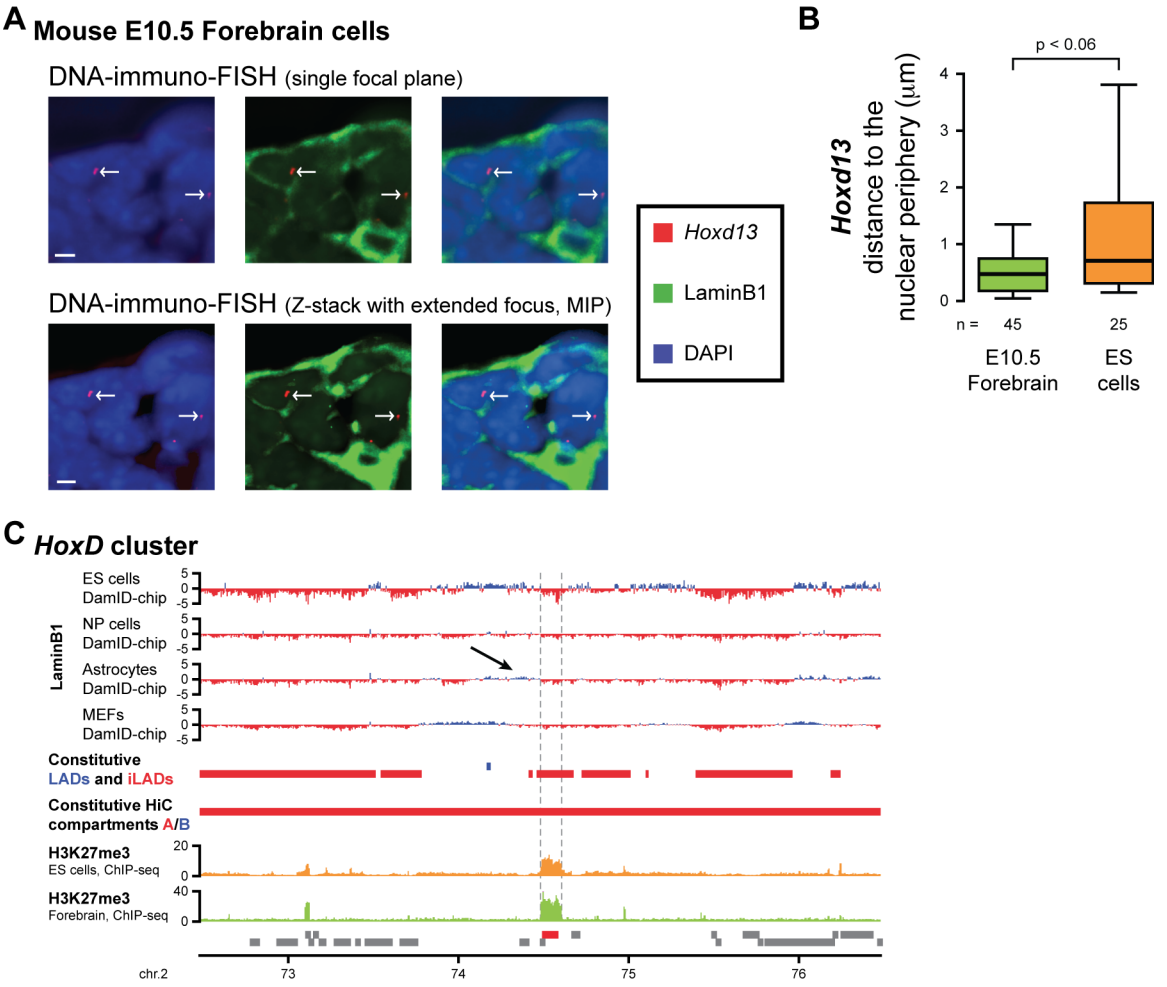

Figure S6. The *HoxD* cluster is located near the nuclear periphery, yet outside of the LaminB1 territory.

(A) DNA-immuno-FISH showing the nuclear position of the *Hoxd13* locus (red), together with the LaminB1 protein (green) in E10.5 forebrain cells. DAPI stain is in blue. The upper panels show one focal plane whereas the lower panels show the extended focus of the full Z-stack, using maximal intensity projection (MIP). The majority of *Hoxd13* signals was located near the nuclear periphery, yet it never overlapped with the strong LaminB1 signal.

(B) Box plot showing the distances between the *Hoxd13* locus and the nuclear periphery in both E10.5 forebrain and ES cells. Statistical significance was assesed using an unpaired t-test.

(C) Mapping of published LaminB1 signals from four cell types (8) within a 4 Mb region around the *HoxD* cluster. The *HoxD* cluster (demarcated by dashed grey lines) is H3K27me3-marked in ES cells and E10.5 forebrain cells (ChIP-seq patterns) and is consistently depleted for LaminB1 signal, confirming its status of iLAD. In contrast, the region directly upstream of the *HoxD* cluster (including the *Lnp* gene) is enriched for LaminB1 signal in astrocytes (arrow) and, to some extent, in ES cells. This upstream LAD may tether the *HoxD* cluster close to the nuclear periphery. The genomic positions and genes are indicated below, with the *HoxD* cluster indicated in red.

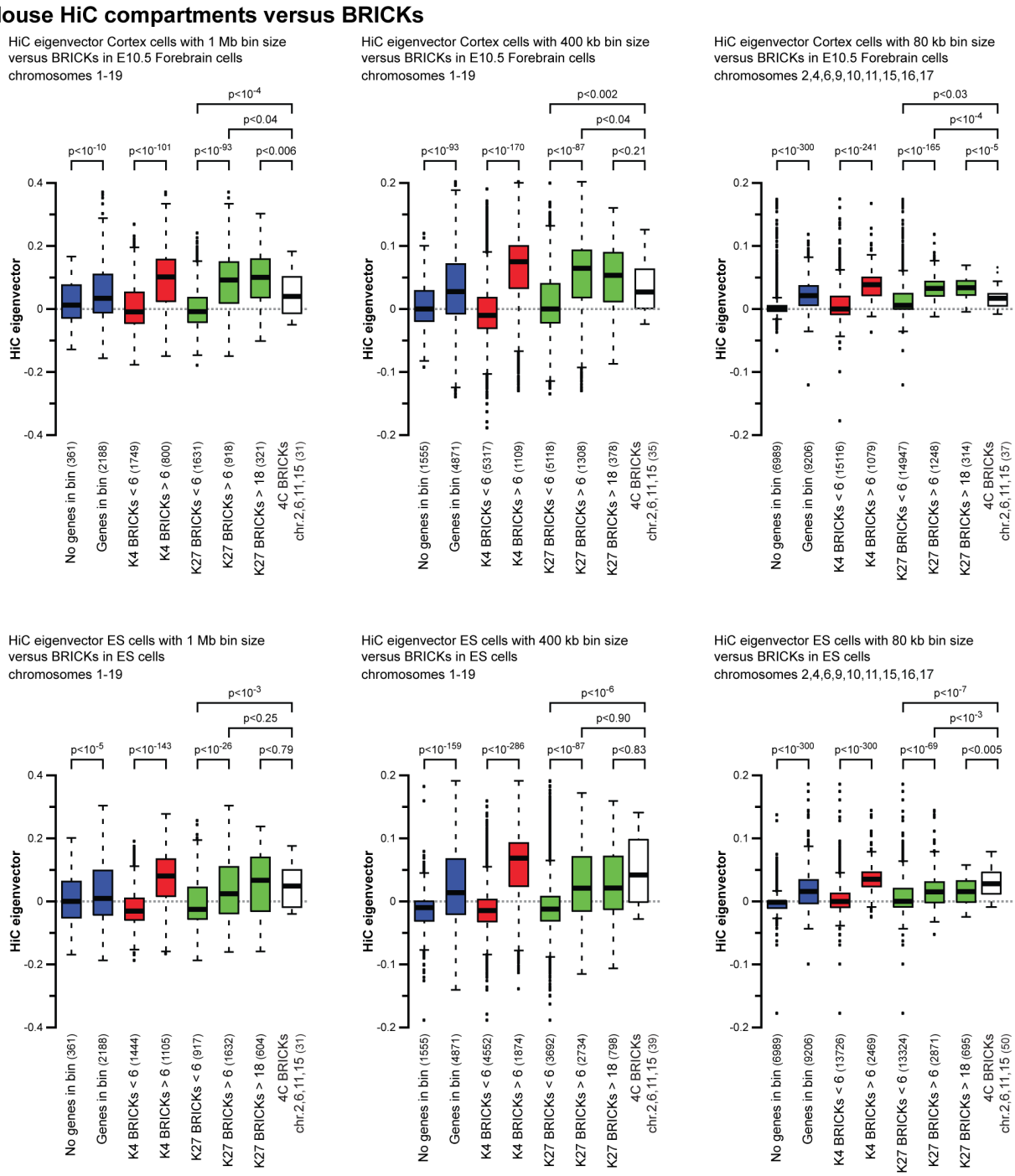

Figure S7. Significant H3K27me3-marked regions and associated 4C-seq interactions are enriched within the active nuclear HiC compartment A, independent of bin-size.

HiC bins at 1 Mb, 400 kb and 80 kb resolutions, in either cortex (top) or ES (bottom) cells were scored either for the presence or absence of genes, for significant domains of histone modifications (K4 or K27 BRICKs) or for significant intra-chromosomal 4C-seq interactions (4C BRICKs). Cortex cell HiC bins were scored *versus* BRICKs from E10.5 forebrain cells and ES cells HiC bins were scored *versus* ES cell BRICKs. See supplemental data file S8 for source of external data.

Bins that contain genes or significant K4 BRICKs (associated with active transcription) consistently show on average a positive HiC eigenvector that is significantly higher than their counterparts that do not match these categories. These results confirm that the HiC compartment A, as described by a positive HiC eigenvector, is indeed the compartment associated with the active transcriptional state.

Moreover, HiC bins that contain significant K27 BRICKS (associated with facultative repression) and bins that are involved in intra-chromosomal interactions between significant K27 BRICKS, show on average a positive sign, which is significantly higher than their counterparts that do not match these categories. Therefore, repressed genes that are labeled by the H3K27me3 mark primarily reside within the active HiC compartment A, where they interact with intra-chromosomal partners. In contrast to a previous HiC study on human cells (7), our BRICK-based analysis detects the enrichment of H3K27me3-marked domains in the active compartment A, and this at all analyzed resolutions, including the highest (80 kb). We therefore conclude that genes repressed by the facultative repressive H3K27me3 mark reside within an active nuclear environment.

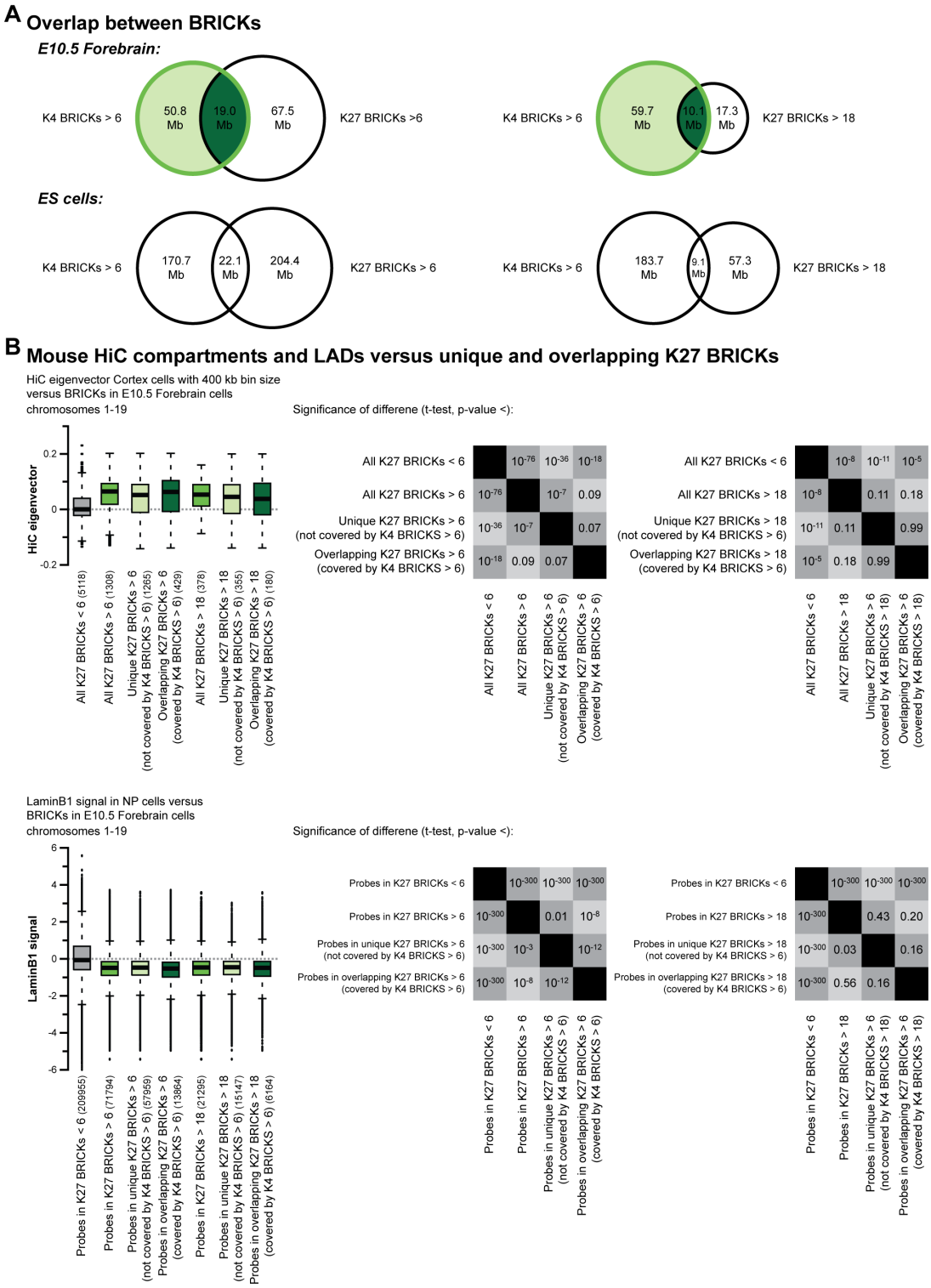

Figure S8. Enrichment of significant H3K27me3-marked regions in the active nuclear HiC compartment A and in iLADs does not depend on a (partial) overlap with H3K4me3 marked-regions.

(A) Venn-diagrams showing overlap and separation between significant K4 and K27 BRICKs. Though K4 and K27 BRICKs (left all significant K27 BIRCKs, right most significant K27 BRICKs) overlap to a certain degree in both cell types (top: E10.5 forebrain cells, bottom ES cells), the majority of the covered regions are unique to K27 BRICKs.

(B) Unique and overlapping categories of K4 and K27 BRICKs in E10.5 forebrain were scored for the overlap with HiC bins (top: cortex cells, 400 kb resolution; similar to Figure S7) and LaminB1 probes (bottom: Neuronal Precursor cells; similar to Figure S8). For ease of interpretation, the shading of box plots corresponds to the surface or outline of the Venn diagrams in panel (A). For all categories of significant K27 BRICKs (all K27 BRICKs combined, unique K27 BRICKs that do not overlap K4 BRICKs or K27 BRICKs that overlap significant K4 BRICKs) consistently the average Eigenvector is positive and the LaminB1 signal is negative. The observed enrichment of the K27 BRICKs in the active HiC compartment A and in the iLADs is therefore not dependent, or solely caused by, the overlap between significant K27 and K4 BRICKs.

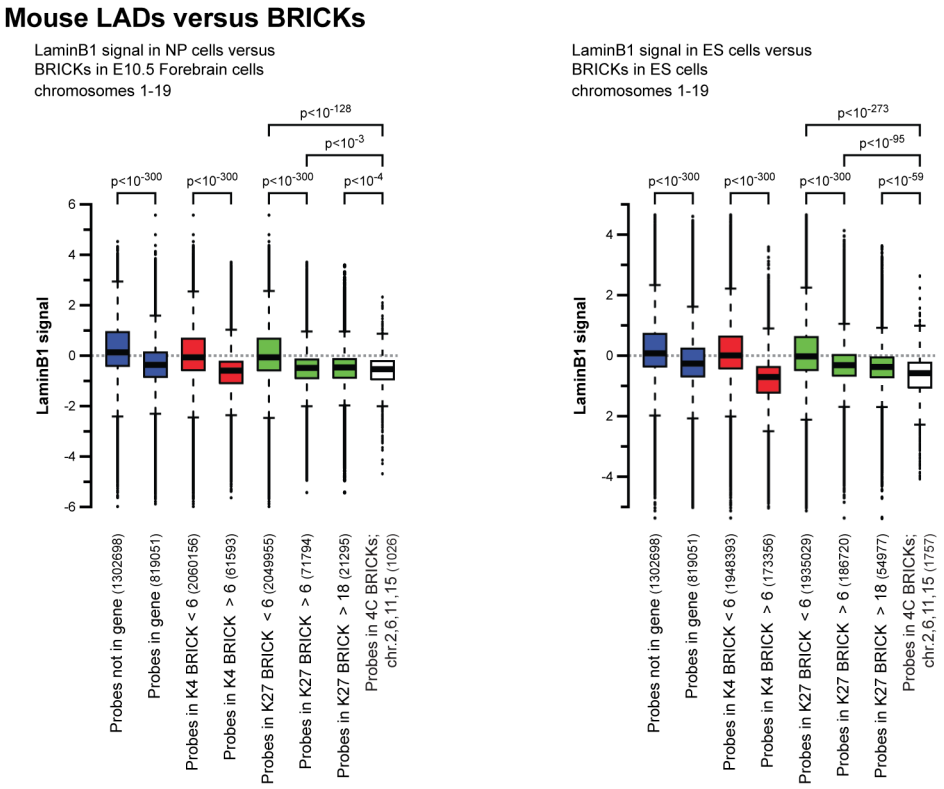

Figure S9. Significant H3K27me3-marked regions and associated 4C-seq interactions are depleted for LaminB1 signal and thus occur primarily in the iLADs.

LaminB1 probes either in Neuronal Precursor (NP) (left) or in ES (right) cells were scored for their overlap either with genes, with significant domains of histone modifications (K4 or K27 BRICKs) or with significant intra-chromosomal 4C-seq interactions (4C BRICKs). LaminB1 probes in NP cells were scored *versus* BRICKs from E10.5 forebrain cells and ES cell probes were scored *versus* ES cell BRICKs. See supplemental data file S8 for source of external data. LaminB1 probes that cover genes or significant K4 BRICKs (associated with active transcription) are generally depleted for LaminB1 signal (i.e. they have a negative log(10) LaminB1 signal), fitting with the idea that inter-Lamina-Associated Domains (iLADs) constitute the active nuclear environment. Moreover, the LaminB1 probes that cover significant K27 BRICKS (associated with facultative repression) and bins that are involved in intra-chromosomal interactions between significant K27 BRICKS have on average a negative log(10) LaminB1 sign. Therefore, repression of genes by the Polycomb group proteins (associated with the H3K27me3 mark) seem to primarily occur in the active iLADs without direct involvement of the nuclear lamina.

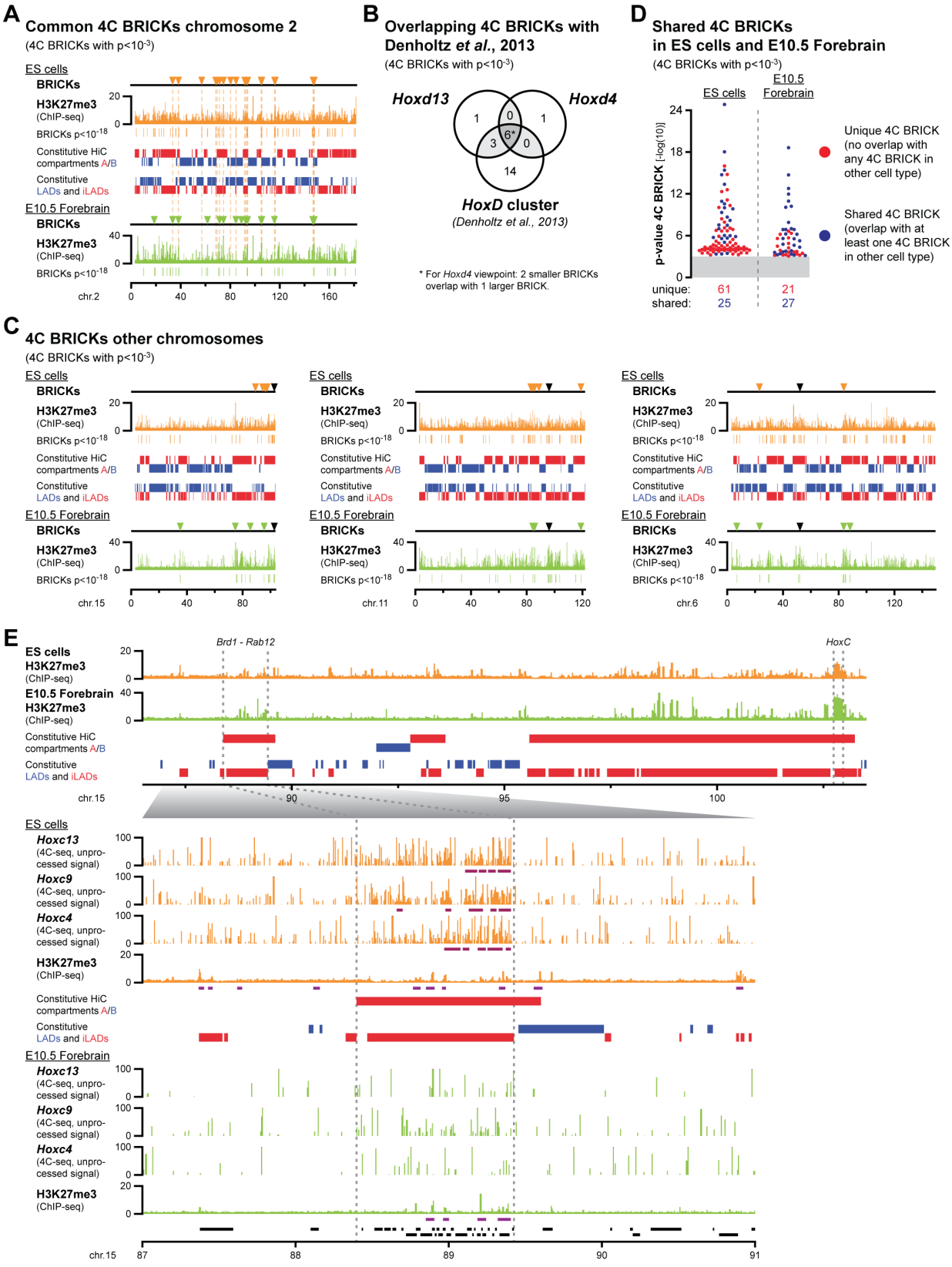

Figure S10. Networks of H3K27me3-associated interactions are also present in ES cells and are moderately reorganized over the course of embryonic development.

(A) Linear visualization of long-range intra-chromosomal 4C-seq interactions on chromosome 2 for four combined viewpoints in ES cells (orange) and E10.5 forebrain cells (green; see supplemental data file S1 for an overview of 4C BRICKs). H3K27me3 ChIP-seq signals and the most significant

enriched regions (BRICKs with p-value < 10^{-18}) are indicated below each profile. Constitutive HiC compartments, LADs and iLADs are indicated in-between and the genomic positions are indicated below. Despite a moderate reorganization, these intra-chromosomal interactions in both cell types primarily occur within the active HiC compartment A (positive, red signal), and the iLADs (negative, red signal).

(B) Comparison of intra-chromosomal interactions in ES cells from the *Hoxd13* and *Hoxd4* viewpoints with a recent, lower-resolution study (17), confirms a large degree of overlap between both datasets.

(C) Comparison of long-range intra-chromosomal 4C-seq interactions of three viewpoints in each of the other *Hox* clusters in ES cells and E10.5 forebrain (significant 4C BRICKs; see supplemental data file S1). Similar to the viewpoints on chromosome 2, each of the other *Hox* clusters contact multiple H3K27me3-marked loci on the same chromosome, which are generally located within the constitutive HiC compartment A (represented by positive red signal) and iLADs (represented by negative red signal). These interactions are moderately reorganized between ES cells and E10.5 forebrain cells. The location of *Hox* clusters is indicated by black arrowheads and the genomic positions are indicated below.

(D) Many significant long-range intra-chromosomal 4C-seq interactions are shared between ES cells and E10.5 forebrain cells, with a tendency for more significant 4C BRICKs to be shared. Shared 4C BRICKs are defined as overlapping with at least one significant 4C BRICK originating from any viewpoint in the other cell type, whereas unique 4C BRICKs do not overlap with any significant 4C BRICK in the other cell type.

(E) Chromatin characteristics of the *Brd1–Rab12* region, a frequent significant interaction partner of the 13 Mb distant *HoxC* cluster in ES cells but not in E10.5 forebrain cells. Top: distribution of the H3K27me3 mark and constitutive HiC, LADs and iLADs in the 15 Mb region upstream of the *HoxC* cluster. The *Brd1–Rab12* gene-dense region and the *HoxC* cluster are indicated above and the genomic positions are shown below. Bottom: magnification of the four Mb around the *Brd–Rab12* region. Unprocessed 4C-seq signal and distribution of the H3K27me3 mark and constitutive HiC, LADs and iLADs are given. Below 4C-seq and ChIP-seq patterns, significant BRICKs are indicated by purple bars. The *Brd1–Rab12* region is the first large constitutive HiC compartment A / iLAD upstream of the *HoxC* cluster. Combined with the presence of several low-significant K27 BRICKs (p-values between 10^{-6} and 10^{-14} in both ES and forebrain cells) and the overall chromatin characteristics of the ES cell genome (see Figure S12), this may allow the formation of detectable long-range interactions between the *HoxC* cluster and this gene-dense, housekeeping gene region.

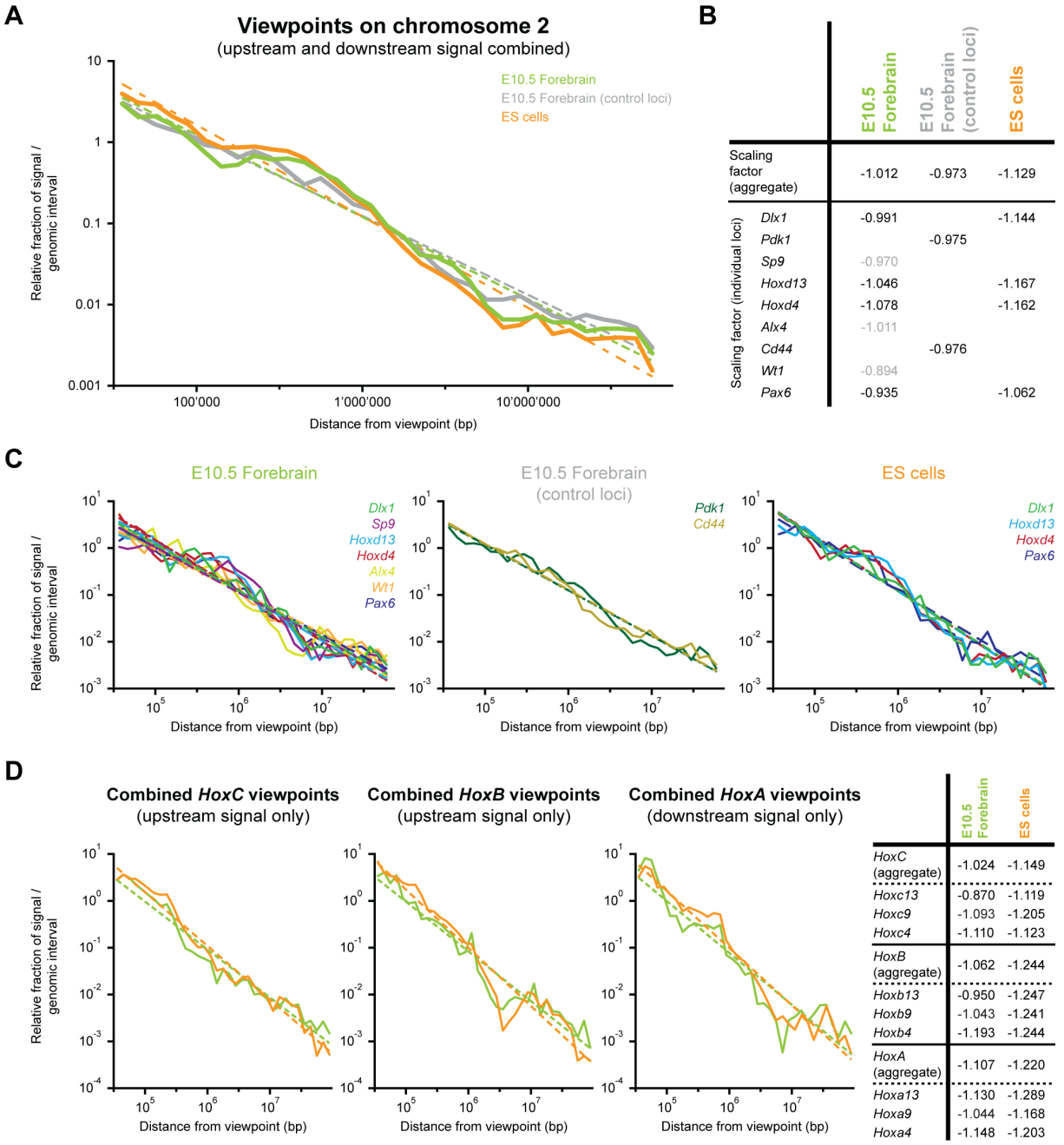

Figure S11. Determination of global scaling patterns from 4C data in both ES and E10.5 forebrain cells reveals that interactions have a chromosome specific pattern with signals in ES cells being more proximal.

(A) Global 4C interactions *versus* distance from the viewpoint on chromosome 2 (see full methods section in this supplement) for four combined H3K27me3-marked viewpoints (green) and two combined non-H3K27me3-marked viewpoints (grey) in E10.5 forebrain and four combined H3K27me3-marked viewpoints (orange) in ES cells. Solid lines indicate the signal per bin, whereas the dashed lines represent the linear fitted curve used to determine the scaling factor.

(B) Scaling factors for different viewpoints on chromosome 2 in ES cells and E10.5 forebrain. Viewpoints used for the aggregate value indicated on top, and for the graph in panel A, are indicated in black, whereas the viewpoints not used for calculations are shown in grey. Consistent for all H3K27me3-marked viewpoints, the scaling factor in ES cells has a larger negative value than in E10.5 forebrain, showing that it is enriched for more proximal interactions and depleted for

more distal interactions in ES cells, supporting a similar conclusion obtained from a recent reanalysis of human HiC data (14). No substantial difference is observed between H3K27me3-marked and non-H3K27me3-marked viewpoints in E10.5 forebrain cells, suggesting that the global organization is independent of the presence of this histone mark.

(C) Global 4C interactions *versus* distance from the viewpoint on chromosome 2 for individual viewpoints. Solid lines indicate the actual signal per bin, whereas the dashed lines represent the linear fitted curve used to determine the scaling factor.

(D) Global 4C interactions *versus* distance from the viewpoint for combined viewpoints in *Hox* clusters on other chromosomes. Solid lines indicate the actual signal per bin, whereas dashed lines represent the linear fitted curve used to determine the scaling factor. Scaling factors for combined and individual viewpoints are shown on the right. Consistent with the results obtained with chromosome 2, the scaling factor in ES cells has a larger negative value than in E10.5 forebrain. Between each chromosome, a certain degree of variation can be observed, supporting a previous report that individual chromosomes display specific folding characteristics (14).

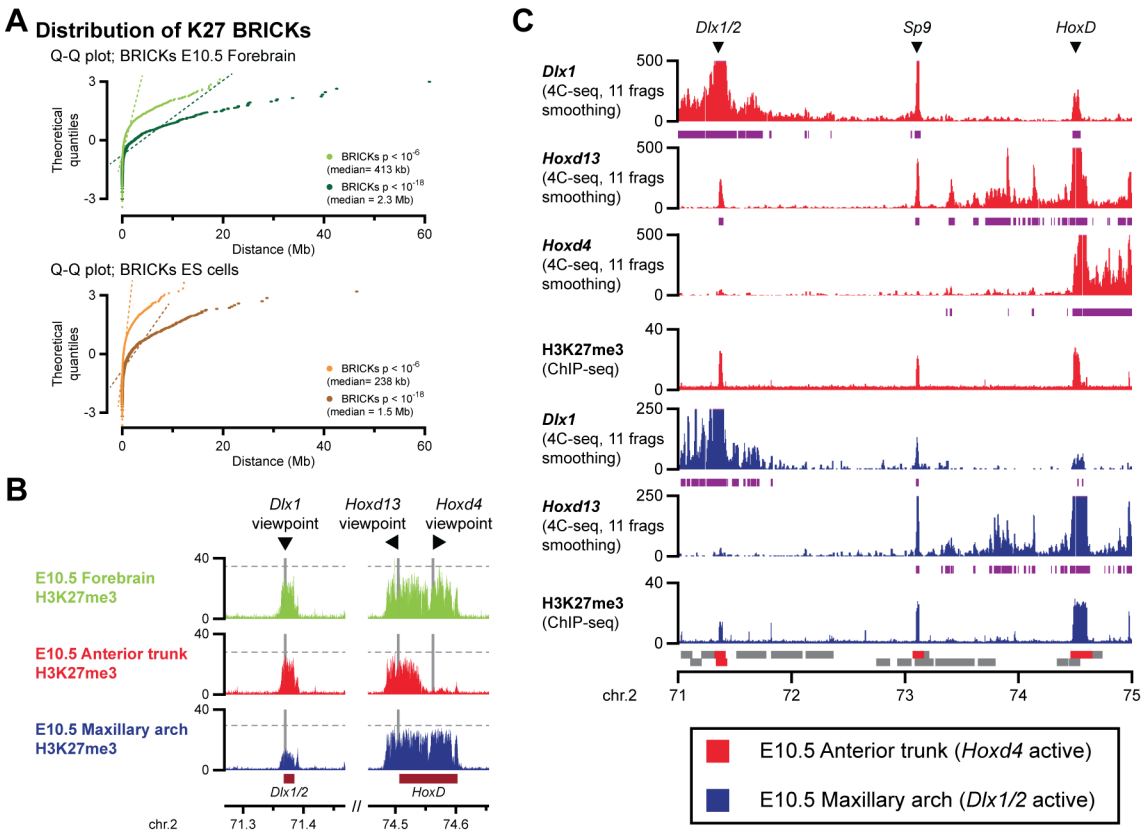

Figure S12. Long-range intra-chromosomal interactions are lost upon transcriptional activation and removal of H3K27me3 marks.

(A) Q-Q (quantile-quantile) plot of distances between significant K27 BRICKs on chromosomes 1 to 19 ($p<10^{-6}$ and $p<10^{-18}$). The dashed line connects the first and third quantile. The strong deviation of the signal from the linear trend confirms that K27 BRICKs are not normally distributed in the genome, at both significance cut-offs.

(B) Zoom into the H3K27me3 ChIP-seq signal on the viewpoints in this analysis. In E10.5 forebrain, large domains of the H3K27me3 mark cover all viewpoints. In E10.5 anterior trunk, the H3K27me3 mark is mostly removed from the *Hoxd4* viewpoint. In E10.5 maxillary arch, the H3K27me3 is strongly reduced from the *Dlx1* viewpoint. The dashed grey line indicates the approximate maximum level of H3K27me3 level at the *HoxD* cluster in each sample. Position of the *Dlx1/2* and *HoxD* cluster and genomic position are indicated below.

(C) Smoothed 4C signal in a four Mb interval on chromosome 2 in tissues where the *Hoxd4* or *Dlx1* gene have been activated (see legend below patterns). Purple bars below the 4C-seq patterns indicate the signal with values within the 80% percentile. Position of the *Dlx1/2* cluster, the *Sp9* gene and the *HoxD* cluster are indicated on top (black arrowheads). The 4C viewpoints are indicated on the right and genomic locations and genes are indicated below, with the *Dlx1/2* cluster, the *Sp9* gene and the *HoxD* cluster indicated in red. In the E10.5 anterior trunk sample, the H3K27me3-marked *Hoxd13* and *Dlx1* genes maintain their interactions, whereas distant interactions of the active *Hoxd4* gene are lost. In the E10.5 maxillary arch sample, where the *Dlx1* gene is active in a majority of cells, the interactions between the *Sp9* and *HoxD* cluster remain, whereas interaction with the *Dlx1/2* cluster are substantially reduced.

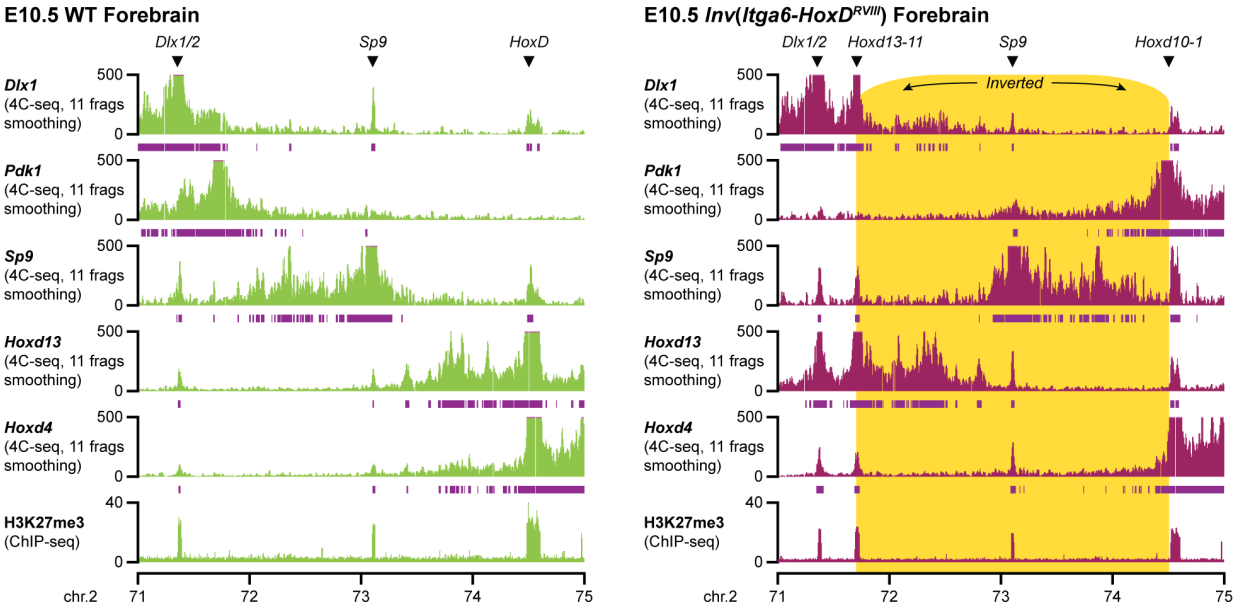

Figure S13. An engineered inversion involving the *HoxD* cluster reveals that long-range contacts are established independently.

Smoothed 4C signal in a four Mb interval on chromosome 2 in E10.5 control forebrain (green, left) and in E10.5 Inv(*Itga6-HoxD*^{RVIII}) mutant forebrain for the *Dlx1*, *Pdk1*, *Sp9*, *Hoxd13* and *Hoxd4*. Except for the *Pdk1* viewpoint, all viewpoints are H3K27me3 marked. Purple bars below 4C-seq patterns indicate signal with values within the 80% percentile. The positions of the *Dlx1/2* cluster, the *Sp9* gene and the *HoxD* cluster, or its two split counterparts generated by the inversion, are indicated above. After inversion, the *Hoxd13* viewpoint strongly contacts the nearby *Dlx1/2* cluster, whereas a severely reduced signal is detected with the *Hoxd10* to *Hoxd1* region. Other H3K27me3-marked viewpoints within the four Mb region contact the repositioned *Hoxd13* to *Hoxd11* region, but otherwise little reorganization of long-range contacts is observed.

Supplemental tables

Table S1. Primers and probes

4C-seq inverse primers

Viewpoint	Inverse primer	Sequence
Hoxd13	iHoxd13 forward*	AATGATACGGCGACCACCGAACACTCTTTCCCTACACGACGCTCTTCCGATCTAAAAATCCTAGACCTGGTCATG
	iHoxd13 reverse*	CAAGCAGAAGACGGCATACGAGGCCGATGGTGCTGTATAGG
Hoxd4	iHoxd4 forward*	AATGATACGGCGACCACCGAACACTCTTTCCCTACACGACGCTCTTCCGATCTAAGGACAATAAAGCATCCATAGGCG
	iHoxd4 reverse*	CAAGCAGAAGACGGCATACGATCCAGTGGAATTGGGTGGGAT
Dlx1	iDlx1 forward*	AATGATACGGCGACCACCGAACACTCTTTCCCTACACGACGCTCTTCCGATCTAAATTACCGAGACTAATACGTGCACA
	iDlx1 reverse*	CAAGCAGAAGACGGCATACGAGTGCGCTTTAACGGCAAAGG
Pdk1	iPdk1 forward	AATGATACGGCGACCACCGAACACTCTTTCCCTACACGACGCTCTTCCGATCTAATTCCAACTGCTCAGTACAACCA
	iPdk1 reverse	CAAGCAGAAGACGGCATACGACAGGCTAGCCCCAAACACAA
Sp9	iSp9 forward	AATGATACGGCGACCACCGAACACTCTTTCCCTACACGACGCTCTTCCGATCTAACGGGAGGCGAGGTCCAT
	iSp9 reverse	CAAGCAGAAGACGGCATACGACAGAGACAGCGCGCAGAG
Alx4	iAlx4 forward	AATGATACGGCGACCACCGAACACTCTTTCCCTACACGACGCTCTTCCGATCTAAAGCCTGAGGACACAGGTGA
	iAlx4 reverse	CAAGCAGAAGACGGCATACGATAGGCGCTTGACTGGCTTTG
Cd44	iCd44 forward	AATGATACGGCGACCACCGAACACTCTTTCCCTACACGACGCTCTTCCGATCTAAGGCACTACACCCCAATCTTCA
	iCd44 reverse	CAAGCAGAAGACGGCATACGATAGGCATTGCTTTCCAGCGG
Wt1	iWt1 forward	AATGATACGGCGACCACCGAACACTCTTTCCCTACACGACGCTCTTCCGATCTAGTTCAGGTCCCGCACGTC
	iWt1 reverse	CAAGCAGAAGACGGCATACGAAAGAGCTTGGTGCCTTTGCA
Pax6	iPax6 forward	AATGATACGGCGACCACCGAACACTCTTTCCCTACACGACGCTCTTCCGATCTAAGGGGGAGGGGATGTCTTTG
	iPax6 reverse	CAAGCAGAAGACGGCATACGATTCTCAAAGCCGCTTCTCGG
Hoxc13	iHoxc13 forward*	AATGATACGGCGACCACCGAACACTCTTTCCCTACACGACGCTCTTCCGATCTAGATAATTTTCCTGAGACATTGTAAC
	iHoxc13 reverse*	CAAGCAGAAGACGGCATACGAGCTCAATGTTCCCTTCCCTAACG
Hoxc9	iHoxc9 forward*	AATGATACGGCGACCACCGAACACTCTTTCCCTACACGACGCTCTTCCGATCTATTCCCCGGGCGAGCCGTACAT
	iHoxc9 reverse*	CAAGCAGAAGACGGCATACGAGTGTCCACAGGAGAGAAGGAGT
Hoxc4	iHoxc4 forward*	AATGATACGGCGACCACCGAACACTCTTTCCCTACACGACGCTCTTCCGATCTACAACAACAAAAACCCAGCAGGT
	iHoxc4 reverse*	CAAGCAGAAGACGGCATACGATGATGTGAAATGCCCCGTGA
Hoxb13	iHoxb13 forward*	AATGATACGGCGACCACCGAACACTCTTTCCCTACACGACGCTCTTCCGATCTAGGACTGTTCCTCGGGGCTAT
	iHoxb13 reverse*	CAAGCAGAAGACGGCATACGAATCTGGCGTTCAGAGAGGCT
Hoxb9	iHoxb9 forward*	AATGATACGGCGACCACCGAACACTCTTTCCCTACACGACGCTCTTCCGATCTAAGATTGAGGAGTCTGGCCACTT
	iHoxb9 reverse*	CAAGCAGAAGACGGCATACGATCATCAAACCAAGCAGGGCA
Hoxb4	iHoxb4 forward*	AATGATACGGCGACCACCGAACACTCTTTCCCTACACGACGCTCTTCCGATCTATCACACGCACAAGAACACCC
	iHoxb4 reverse*	CAAGCAGAAGACGGCATACGACTCCCCGAATTAGTGCGTGAAT
Hoxa13	iHoxa13 forward*	AATGATACGGCGACCACCGAACACTCTTTCCCTACACGACGCTCTTCCGATCTAACACTTGCACAACCAGAAATGC
	iHoxa13 reverse*	CAAGCAGAAGACGGCATACGAGGCGAGGCTCAGGCTTTTAT
Hoxa9	iHoxa9 forward*	AATGATACGGCGACCACCGAACACTCTTTCCCTACACGACGCTCTTCCGATCTAGGGATGCATAGATTCATG
	iHoxa9 reverse*	CAAGCAGAAGACGGCATACGAACAGTGTTCAAGTATTTTGG
Hoxa4	iHoxa4 forward*	AATGATACGGCGACCACCGAACACTCTTTCCCTACACGACGCTCTTCCGATCTAGCAAGGAGAGGAAACTAC
	iHoxa4 reverse*	CAAGCAGAAGACGGCATACGAGTGGTGTTACTGTGCACTC

Location of primers according to NCBI37 (mm9).

* Primers from: Noordermeer D., *et al.*, The dynamic architecture of *Hox* gene clusters **2011** Science *334*, 222-225.

DNA-FISH probes

Region	Name	Start	End	Size (bp)
Hoxd13	WI1-469P2 (Fosmid)	74636100	74674945	38845
Alx4	CH29-163J23 (BAC)	93468017	93667967	199950
Cd44	CH29-1O14 (BAC)	102882509	103134265	251756
Pax6	WI1-126M19 (Fosmid)	105672291	105712637	40346

Location of probes according to NCBI37 (mm9).

Table S2. Public datasets used in this study

Dataset	Accession	Reference
H3K27me3 mouse ES cells (ChIP-seq)	GSM1327220	Noordermeer D., *et al.*, Temporal dynamics and developmental memory of 3D chromatin architecture at *Hox* gene loci **2014** eLife *3*, e02557
H3K4me3 mouse ES cells (ChIP-seq)	GSM1327219	Noordermeer D., *et al.*, Temporal dynamics and developmental memory of 3D chromatin architecture at *Hox* gene loci **2014** eLife *3*, e02557
H3K4me3 mouse E10.5 Forebrain cells (ChIP-seq)	GSM783882	Noordermeer D., *et al.*, The dynamic architecture of *Hox* gene clusters **2011** Science *334*, 222-225
H3K4me3 mouse cortex cells (ChIP-seq)	GSM769026	Shen Y., et al., A map of the *cis*-regulatory sequences in the mouse genome **2012** Nature *488*, 116–120
Mouse HiC data (normalized matrices for ES cells and Cortex cells)	http://yuelab.org/hi-c/download.html	Dixon J.R., *et al.*, Topological domains in mammalian genomes identified by analysis of chromatin interactions. **2012** Nature *485,* 376-380
LaminB1 mouse ES cells (DamID-chip)	GSM426758 and GSM426759	Peric-Hupkes, D., *et al.*, Molecular Maps of the Reorganization of Genome-Nuclear Lamina Interactions during Differentiation **2010** Mol Cell *38*, 603-613
LaminB1 mouse NPC cells (DamID-chip)	GSM426760 and GSM426761	Peric-Hupkes, D., *et al.*, Molecular Maps of the Reorganization of Genome-Nuclear Lamina Interactions during Differentiation **2010** Mol Cell *38*, 603-613
LaminB1 mouse Astrocytes (DamID-chip)	GSM426762 and GSM426763	Peric-Hupkes, D., *et al.*, Molecular Maps of the Reorganization of Genome-Nuclear Lamina Interactions during Differentiation **2010** Mol Cell *38*, 603-613
LaminB1 mouse NIH3T3 cells (DamID-chip)	GSM426764 and GSM426765	Peric-Hupkes, D., *et al.*, Molecular Maps of the Reorganization of Genome-Nuclear Lamina Interactions during Differentiation **2010** Mol Cell *38*, 603-613
Constitutive LADs and iLADs	GSE17051	Meuleman, W., *et al.*, Constitutive nuclear lamina–genome interactions are highly conserved and associated with A/T-rich sequence **2013** Genome Res *23*, 270-280

Description of supplemental files

File S1. Intra-chromosomal 4C BRICKs

Microsoft Excel file containing intra-chromosomal BRICKs identified in E10.5 wild-type forebrain cells, E10.5 wild-type junction cells, wild-type ES cells, E10.5 wild-type anterior trunk cells, E10.5 wild-type maxillary arch cells and E10.5 Inv(*Itga6-HoxD*^{RVIII}) mutant forebrain cells.

File S2. Inter-chromosomal 4C BRICKs

Microsoft Excel file containing inter-chromosomal BRICKs identified in E10.5 wild-type forebrain cells.

File S3. H3K27me3 BRICKs.

Microsoft Excel file containing H3K27me3 BRICKs identified in E10.5 wild-type forebrains cells, wild-type ES cells, E10.5 wild-type anterior trunk cells, E10.5 wild-type junction cells, E10.5 wild-type maxillary arch cells and E10.5 Inv(*Itga6-HoxD*^{RVIII}) mutant forebrain cells.

File S4. H3K4me3 BRICKs

Microsoft Excel file containing H3K4me3 BRICKs identified in E10.5 wild-type forebrain cells and wild-type ES cells.

File S5. Constitutive HiC compartments

BedGraph containing coordinates of constitutive HiC compartments at a 400 kb resolution. Coordinates were obtained after intersecting HiC compartment data from mouse ES cells and cortex cells, which were generated by reanalysis of previously published data (5). A value of 1 refers to the active HiC compartment A, whereas a value of -1 refers to the inactive HiC compartment B.

Supplemental references

1. Spitz F, Herkenne C, Morris MA, & Duboule D (2005) Inversion-induced disruption of the Hoxd cluster leads to the partition of regulatory landscapes. *Nat Genet* 37(8):889-893.
2. Noordermeer D*, et al.* (2011) The dynamic architecture of Hox gene clusters. *Science* 334(6053):222-225.
3. Noordermeer D*, et al.* (2014) Temporal dynamics and developmental memory of 3D chromatin architecture at Hox gene loci. *eLife* 3:e02557.
4. David FP*, et al.* (2014) HTSstation: A Web Application and Open-Access Libraries for High-Throughput Sequencing Data Analysis. *PLoS One* 9(1):e85879.
5. Dixon JR*, et al.* (2012) Topological domains in mammalian genomes identified by analysis of chromatin interactions. *Nature* 485(7398):376-380.
6. Shen Y*, et al.* (2012) A map of the cis-regulatory sequences in the mouse genome. *Nature* 488(7409):116-120.
7. Lieberman-Aiden E*, et al.* (2009) Comprehensive mapping of long-range interactions reveals folding principles of the human genome. *Science* 326(5950):289-293.
8. Peric-Hupkes D*, et al.* (2010) Molecular maps of the reorganization of genome-nuclear lamina interactions during differentiation. *Molecular cell* 38(4):603-613.
9. Meuleman W*, et al.* (2013) Constitutive nuclear lamina-genome interactions are highly conserved and associated with A/T-rich sequence. *Genome Res* 23(2):270-280.
10. Morey C, Da Silva NR, Perry P, & Bickmore WA (2007) Nuclear reorganisation and chromatin decondensation are conserved, but distinct, mechanisms linked to Hox gene activation. *Development* 134(5):909-919.
11. de Wit E, Braunschweig U, Greil F, Bussemaker HJ, & van Steensel B (2008) Global chromatin domain organization of the Drosophila genome. *PLoS Genet* 4(3):e1000045.
12. Noordermeer D*, et al.* (2011) Variegated gene expression caused by cell-specific long-range DNA interactions. *Nat Cell Biol* 13(8):944-951.
13. Splinter E*, et al.* (2011) The inactive X chromosome adopts a unique three-dimensional conformation that is dependent on Xist RNA. *Genes Dev* 25(13):1371-1383.
14. Barbieri M*, et al.* (2012) Complexity of chromatin folding is captured by the strings and binders switch model. *Proc Natl Acad Sci U S A* 109(40):16173-16178.
15. Couly G, Grapin-Botton A, Coltey P, Ruhin B, & Le Douarin NM (1998) Determination of the identity of the derivatives of the cephalic neural crest: incompatibility between Hox gene expression and lower jaw development. *Development* 125(17):3445-3459.
16. Dolle P, Price M, & Duboule D (1992) Expression of the murine Dlx-1 homeobox gene during facial, ocular and limb development. *Differentiation* 49(2):93-99.
17. Denholtz M*, et al.* (2013) Long-range chromatin contacts in embryonic stem cells reveal a role for pluripotency factors and polycomb proteins in genome organization. *Cell Stem Cell* 13(5):602-616.